

Phantom Design Method for High-Field MRI Human Systems

Qing X. Yang,^{1*} Jinghua Wang,¹ Christopher M. Collins,¹ Michael B. Smith,¹ Xiaoliang Zhang,² Kamil Ugurbil,² and Wei Chen²

A phantom design method suitable for high-field MRI based on the RF field wave characteristics of sample and experimental validations at 7.0 T and 3.0 T are presented. The RF field distribution in a phantom with a given RF coil system is primarily determined by the sample size relative to the wavelength inside the sample, and the ratio between the displacement and conduction currents. Experimental results demonstrate that the MR image intensity patterns associated with wave behavior in human samples at a given field strength can be reproduced with a phantom at the same or different field strengths once the dimension and penetration constant are scaled by the corresponding wavelength in the sample medium. Magn Reson Med 52:1016–1020, 2004. © 2004 Wiley-Liss, Inc.

Key words: high-field MRI; RF field; phantom design; RF coil; MRI

The advantages of high-field MRI have led to the proliferation of whole-body, high-field research systems (3–8 T), and worldwide acceptance of 3.0 T systems for standard clinical use (1–11). There has been great interest in advancing the static magnetic field of human MRI systems to even higher strengths. One of the difficulties encountered in high-field MRI systems is the prominent radiofrequency (RF) field inhomogeneity inside physiological samples (11–17). This phenomenon is due to the RF field wave behavior as the wavelength of the RF field becomes comparable to a human-sized sample in the frequency regime of high-field human imaging systems (18).

The RF field and image intensity distributions in a sample are determined by the geometry and electrical properties of the coil-sample configuration. The routinely used water-based phantoms are no longer suitable for high-field MRI applications because their electrical properties and image intensity distribution can significantly differ from those in human samples at high fields (18,19). Thus, for high-field coil design and sequence development, it is

necessary to first understand the basic characteristics of the RF field wave behavior in the human body, and subsequently devise methodologies for phantom design that simulate the RF field distributions in human samples at various frequencies. In addition, it is experimentally and theoretically important to develop a validated method that will allow comparison of image intensity distributions at various static field strengths, and predictions of image intensity distribution at higher field strengths than are currently available. In this report, we present an analysis of the electromagnetic wave inside biological samples, and propose a phantom design method that is based on the sample electrical characteristics in the presence of strong wave behavior. With this approach, the RF field and resultant image intensity distributions in the human body can be simulated more closely, compared at different field strengths, and extrapolated to even higher field strengths.

To validate the theory, we first sought to demonstrate that the phantom designed with our method would closely simulate image intensity distribution in the human brain at 7.0 T. Second, we applied our phantom design method to simulate the RF field in the human brain at 9.4 T with a 7.0 T system.

THEORY

The basic behavior of the RF field in the human brain can be characterized by considering the electromagnetic field in a uniform conducting medium (18,19). In this case, the electromagnetic wave is described with the complex propagation constant γ :

$$\gamma = j\omega \sqrt{\mu \left(\epsilon - j \frac{\sigma}{\omega} \right)} = \alpha + j\beta \quad (\text{m}^{-1}) \quad [1]$$

where $\epsilon = \epsilon_0 \epsilon_r$ is the electric permittivity, μ is the magnetic permeability, σ is conductivity in the media, ω is the resonance angular frequency, and $j = \sqrt{-1}$ is the complex unit (20). The real (α) and imaginary (β) parts of γ are the attenuation and phase constants, respectively, which are expressed as:

$$\alpha = \frac{\omega \sqrt{\mu \epsilon}}{\sqrt{2}} \left[\sqrt{1 + \left(\frac{\sigma}{\omega \epsilon} \right)^2} - 1 \right]^{1/2} \quad [2]$$

$$\beta = \frac{\omega \sqrt{\mu \epsilon}}{\sqrt{2}} \left[\sqrt{1 + \left(\frac{\sigma}{\omega \epsilon} \right)^2} + 1 \right]^{1/2} \quad [3]$$

¹Center for NMR Research, Department of Radiology, Pennsylvania State University College of Medicine, Hershey, Pennsylvania.

²Center for MR Research, Department of Radiology, School of Medicine, University of Minnesota, Minneapolis, Minnesota.

Grant sponsor: Whitaker Foundation; Grant number: RG-99-0157; Grant sponsor: NIH; Grant numbers: RO1 EB00454-01A1; RO1 EB00513; RO1 EB00329; RO1 NS38070; RO1 NS39043; and RO1 P41 RR08079; Grant sponsors: W.M. Keck Foundation; MIND Institute.

*Correspondence to: Qing X. Yang, Center for NMR Research, NMR/MRI Building, Department of Radiology H066, Pennsylvania State University College of Medicine, 500 University Drive, Hershey, PA 17033. E-mail: qyang@psu.edu

Received 19 January 2004; revised 10 June 2004; accepted 10 June 2004.

Published online in Wiley InterScience (www.interscience.wiley.com).DOI 10.1002/mrm.20245

Table 1
The Parameters for Phantom Designs at 3.0, 7.0, and 9.4 T

	Conductivity σ (S/m) ^a	Permittivity ϵ_r ^a	Wavelength λ_e (cm)	Skin depth (cm)	Size L (cm)	Ratio L/ λ	Ratio $\sigma/\omega\epsilon_0\epsilon_r$
7.0 T brain properties	0.657	50.5	13.2	6.12	16.0	1.21	0.776
7.0 T brain phantom	1.015	78.0	10.6	4.92	12.8	1.21	0.776
7.0 T brain phantom equivalent at 3.0 T	0.423	78.0	25.5	11.8	31.0	1.21	0.776
9.4 T brain properties	0.695	47.7	10.4	5.83	16.0	1.54	0.657
9.4 T brain phantom equivalent at 7.0 T	0.853	78.0	10.8	5.76	16.6	1.54	0.657

^aThe brain conductivity and permittivity at 7.0 T and 9.4 T are the average values of gray and white matters at corresponding frequencies (21).

It is important to note that these two quantities depend on the ratio $\sigma/\omega\epsilon$ of the conduction current $j_c = \sigma E$ and the displacement current $j_d = \omega\epsilon E$, where E is the electrical field strength. The wavelength λ and skin depth δ of the RF field in the sample are given by $\lambda = 2\pi/\beta$ and $\delta = 1/\alpha$, respectively. In the above formulas, a decaying plane wave in a homogeneous medium is assumed. Since the conductivity of biological tissues σ generally increases, while the dielectric constant ϵ generally decreases with the electromagnetic field frequency, the ratio $\sigma/\omega\epsilon$ is frequency-dependent (18,21). For example, the ratio is $2.0 > \sigma/\omega\epsilon > 0.67$ for the average of gray and white matter in the frequency range of 50–500 MHz. Thus, the behavior of the RF field in a human sample is expected to differ significantly from that in a water phantom with similar geometric dimensions, because $\sigma/\omega\epsilon < 1$ for water. The rationale for simulation of the RF field wave behavior occurring in the human brain (sample I) with a phantom (sample II) is that both sample sizes L_I and L_{II} and skin-depths δ_I and δ_{II} are scaled by the corresponding RF field wavelength in the sample:

$$\delta_I/\lambda_I = \delta_{II}/\lambda_{II} \quad [4]$$

$$L_I/\lambda_I = L_{II}/\lambda_{II} \quad [5]$$

The relationship in Eq. [4] leads to a simple criterion: $\sigma_I/\omega_I\epsilon_I = \sigma_{II}/\omega_{II}\epsilon_{II}$. This criterion can be satisfied by matching both σ_{II} and ϵ_{II} to the relevant biological sample. This can be achieved experimentally by adding a given amount of NaCl and sucrose. As previously demonstrated, the conductivity and dielectric constant of an aqueous sample can be varied, respectively, with NaCl and sucrose of certain concentrations (22–23). Alternatively, the criterion can be met by varying σ_{II} alone with different concentrations of NaCl aqueous solution while maintaining ϵ_{II} , or vice versa. In this case, the sample size must also be scaled using Eq. [5], since the wavelength of the RF field is dependent on ϵ_r . Although the former approach is more complicated, it is also more advantageous because it more closely simulates the loading effect of the biological sample to the RF coil, and the phantom size can be kept the same as the biological sample dimension. However, the latter approach was adopted for the current phantom design because it is simple to implement and allows for rigorous testing of our theory.

MATERIALS AND METHODS

7.0 T Human Brain Phantom

We created a brain phantom by adjusting σ with the NaCl concentration so that the ratio $\sigma/\omega\epsilon$ was the same as that in brain tissue at 300 MHz. Assuming that the diameter of the brain is roughly 16 cm, we scaled the diameter of the brain phantom to 13 cm to maintain the appropriate ratio of diameter to wavelength at 7.0 T. The parameters for the brain and brain phantom are listed in Table 1. The brain conductivities and permittivities at frequencies corresponding to 7.0 T and 9.4 T shown in Table 1 are the average values of gray and white matters at previously determined corresponding frequencies (21).

Phantoms for Different Field Strengths

The phantom design for different field strengths was first validated with the 7.0 T brain phantom and its equivalent phantom at 3.0 T. Subsequently, prediction of the RF field distribution in a 9.4 T brain phantom was demonstrated with its equivalent phantom at 7.0 T. The parameters for the brain phantoms and their equivalents at different field strengths are also listed in Table 1. Based on the theoretical analysis, the phantoms were designed such that the ratios of L/λ and $\sigma/\omega\epsilon$ of the two phantom pairs at 7.0 T/3.0 T and 9.4 T/7.0 T were kept the same.

To demonstrate the image intensity characteristics of the phantom in the presence of RF field wave behavior, gradient-recalled-echo (GRE) images with small flip angle were used. The intensity of a GRE image depends approximately on the B_1 field strength linearly when the flip angle is small. Phantoms and a human head were imaged with a linear surface coil, a quadrature surface coil, and a TEM volume coil (24) on a 7.0 T human imaging system (MagneX magnet with Varian NMR console) with TR/TE = 1000/5 ms, matrix = 128×128 , FOV = 20×20 cm², and slice thickness = 3 mm. Because of the wave behavior and the use of the surface coil, the RF field was extremely inhomogeneous inside the samples. To set up the proper RF power of the excitation pulse under such circumstances, we first determined a nominal 90° flip angle by the power setting that produced the maximal GRE intensity from the excited slice. Subsequently, we determined a nominal 5.6° flip angle for all of the experimental images by adding 24 dB attenuation to the 90° excitation pulse. Under these experimental conditions, the T_1 modulation on the image intensity distribution was insignificant.

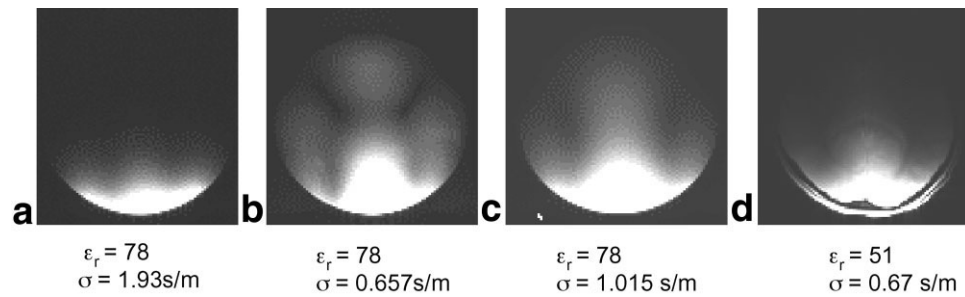


FIG. 1. Axial GRE images at 7.0 T using a surface coil from a 150-mM NaCl (physiological saline) phantom with 16 cm diameter (a), a 50-mM NaCl phantom with 16 cm diameter (b), a 80-mM NaCl phantom with 13 cm diameter (c), and a human head (d). The image intensity distribution of the 80-mM NaCl phantom designed with our method produces an image intensity distribution similar to that in the human brain image. The relative permittivity (ϵ_r) and conductivity (σ) of the sample are listed on the bottom of each image. The image intensities were windowed such that the relative intensity patterns could be observed in the entire sample.

The method of simulating the image intensity distribution of phantom at high field with a lower-field imaging system was validated on phantoms and a human head by means of 7.0 T and 3.0 T human imaging systems (Med-spec S300; Bruker Instruments, Ettlingen, Germany) using identical experimental parameters. With the current method, we subsequently predicted the image intensity distribution in the human head at 9.4 T using experimental images of the equivalent brain phantom at 7.0 T.

RESULTS

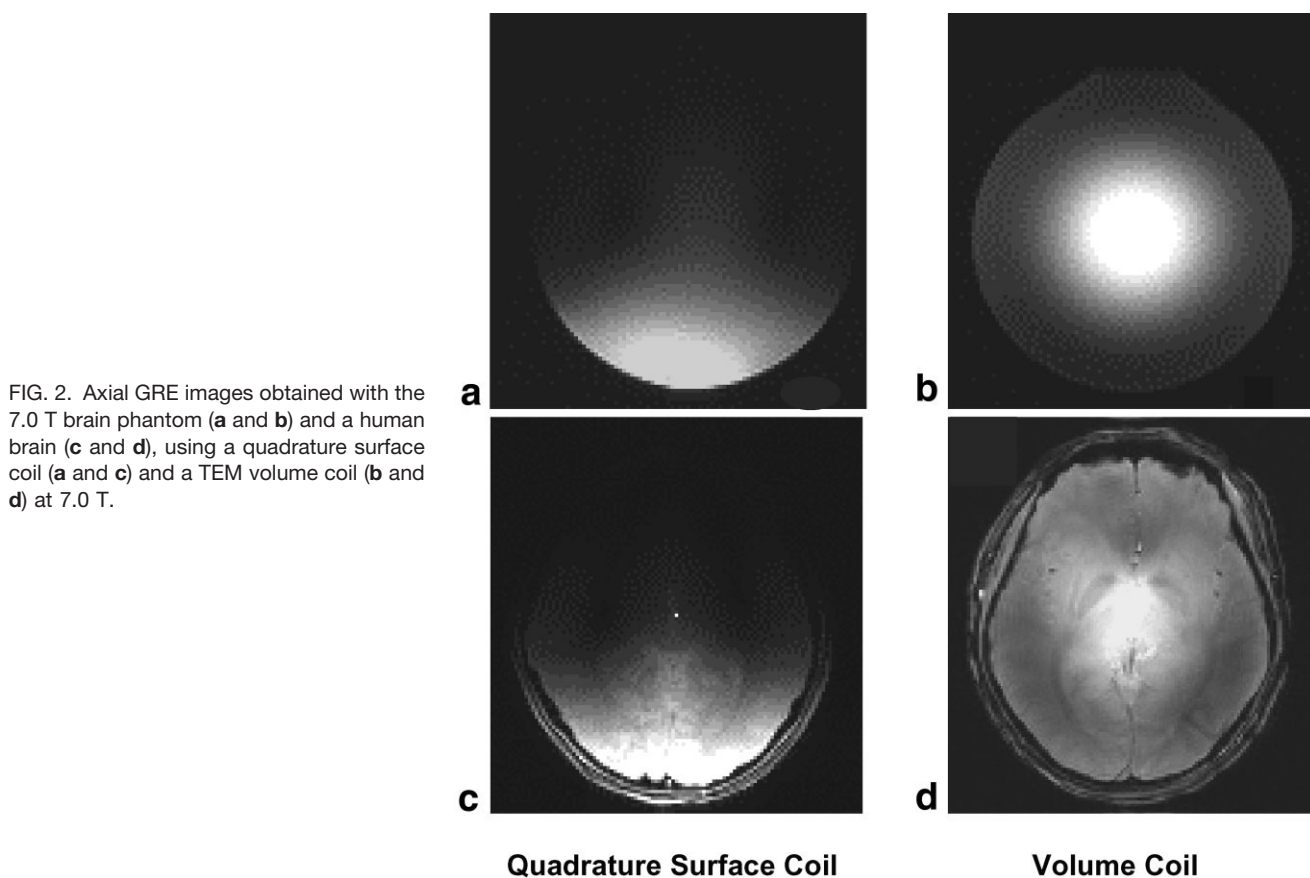
Figure 1 shows an axial human head image acquired at 7.0 T with a linear surface coil, along with images of spherical phantoms in three representative conditions. The image intensity of a 16-cm-diameter physiological saline phantom (150 mM NaCl, $\sigma = 1.96$ S/m, $\epsilon_r = 78$; Fig. 1a) decays rapidly because of its large conductivity. The image intensity pattern of a 50-mM NaCl phantom with the same conductivity (0.657 S/m) as that of average human gray and white matter at 300 MHz (Fig. 1b) is distinctively different from that in the brain image shown in Fig. 1d. The RF field appears to propagate further than that in the brain because of the higher permittivity ($\epsilon_r = 78$) of water. The criteria in Eqs. [4] and [5] were not satisfied in these two cases. The image in Fig. 1c of the brain phantom (80 mM NaCl) that followed our design criteria produced an image intensity distribution similar to that of the human brain in Fig. 1d. The size of the 7.0 T brain phantom image was rescaled to the same size as the images in Fig. 1a and b for comparison purposes. As shown in Fig. 2, the 7.0 T brain phantom also yields an image intensity distribution similar to that produced in a human head with the use of a quadrature surface coil and a TEM volume coil. The specific image intensity patterns of the two dark bands with the quadrature surface coil and the bright center “spot” with the volume coil observed in the human head image were reproduced in the brain phantom image (19). Thus, the image intensity of the brain phantom closely approximates the image distribution in the human brain at 7.0 T. The ratio of image intensity at the center to that at the periphery is greater in the phantom (Fig. 2b) than in the human head (Fig. 2d) when imaged with a volume coil. This difference may be due to the spherical geometry and uniform electrical properties of the phantom: The electri-

cal distance from each element of the volume coil to the center of the phantom is identical when the phantom is imaged, but not when the human head is imaged, allowing for much stronger interference effects in the phantom.

Figure 3 shows the experimental images of the brain phantom acquired at 7.0 T, and its equivalent phantom at 3.0 T obtained with a surface coil. The image intensity pattern at 7.0 T in Fig. 3b is very similar to the experimental image of the equivalent phantom at 3.0 T in Fig. 3a. The agreement in signal distributions in these two experimental images validated that the image intensity pattern associated with the wave behavior at a given field strength could be reproduced at different field strengths following our design criteria. Subsequently, the signal distribution of the human head image at 9.4 T was “experimentally” predicted with an equivalent phantom at 7.0 T following the method shown in Fig. 3c. In this case, the image intensity distribution in the 9.4 T brain phantom yields a w-shaped pattern similar to that seen in a human head at 7.0 T, with a slight reduction in penetration depth (18). The above phantom and human images are presented in axial view because the axial images show more distinctive intensity patterns at a given field strength in a specific sample (18,19). It is most important and straightforward to use axial images to discern the similarities and differences in image intensity distribution with the given sample and coil conditions.

DISCUSSION

In this study we aimed to develop phantoms that characterize basic RF field patterns in the human brain in high-field MRI. Such a phantom design method is essential for developing strategies and methodologies to overcome RF field inhomogeneity problems for high-field systems. This method was developed based on formulas for unbounded electromagnetic waves in a uniform conductive medium. Since the field pattern in a sample can be regarded as a superposition of plane waves subject to given boundary conditions, the fields inside the two samples are identical, provided that the dimensions of the coil-sample configurations and field characteristics are scaled by the wavelength. Figure 1 shows comparisons of the experimental results based on our method with two “rational phantom designs.” In the physiological saline phantom in Fig. 1a, the image intensity is distributed only near the phantom surface area, which indi-



icates that the RF field inside the phantom experienced a stronger attenuation than that in the human head. This is significantly different from the brain image in Fig. 1d because the physiological saline conductivity of the phantom in Fig. 1a was about three times that of the average brain tissue. The RF field distribution of the phantom that matched the brain conductivity in Fig. 1b was very different from that of the brain image in Fig. 1d. The RF field in this phantom appears to penetrate deeper into the sample. The cause for this discrepancy was that the relative permittivity of this phantom was about 50% higher than that of the brain tissue sample, resulting in a stronger displacement current J_d that facilitated RF wave propagation. By matching the ratio $\sigma/\omega\epsilon$ of the phantom with that of the brain tissue, and scaling the phantom size appropriately, we achieved an RF field pattern very similar to that in the brain, as shown in Fig. 1c.

With this approach, the ϵ , σ , and dimensions of the brain phantom are different from those in the human brain, and

only the ratios $\sigma/\omega\epsilon$ and diameter/wavelength are the same as in brain tissue. Thus, the loading effect of the sample to the coil can differ from that of the human head. To simulate the loading effect more closely, both ϵ_r and σ should be matched to those of the brain. Our current approach demonstrates that one can simulate the RF field distribution in the brain by adjusting a single electrical parameter in a phantom using aqueous solutions, when the phantom size is scaled appropriately.

In the presence of wave behavior, the RF field distributions of a coil design at different field strengths are no longer the same. However, it is possible to compare and predict the RF field distributions of a given coil design at different field strengths if the size and skin-depth of the sample are scaled with the corresponding wavelength. Experimental results at 7.0 T and 3.0 T (Fig. 3) validated our method of phantom design for different field strengths, and demonstrated that an RF field distribution in a human-

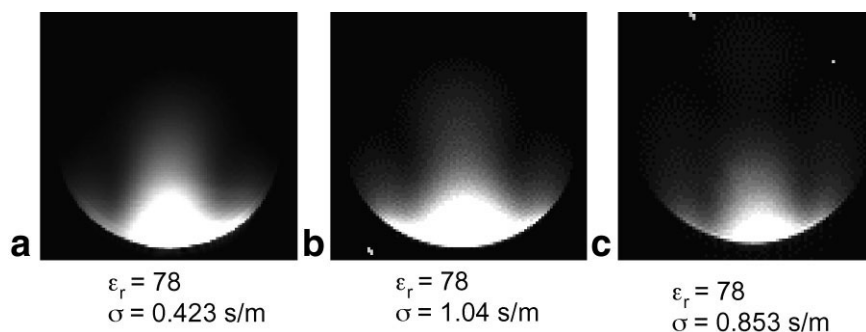


FIG. 3. Axial GRE images with a surface coil of the 7.0 T brain phantom equivalent at 3.0 T, (a) 7.0 T brain phantom, (b) and 9.4 T brain phantom equivalent at 7.0 T. (c) The image of the 7.0 T brain phantom and its equivalent at 3.0 T yield similar intensity patterns at the two field strengths. The simulation of the 9.4 T brain image with the equivalent phantom at 7.0 T indicates that a brain image intensity pattern at 9.4 T would be similar to that at 7.0 T, though with slightly less penetration.

sized sample at high field strength could be produced at lower field strengths. With this method, the RF field behavior at even higher field strengths (which are currently unavailable) can be examined for feasibility studies. The image intensity pattern of the 9.4 T brain phantom predicted by its equivalent at 7.0 T (Fig. 3c) indicates that the RF field in a human head at 9.4 T will produce a pattern similar to that at 7.0 T, with a slight reduction in penetration depth. This is because the “skin depth” of biological tissues (listed in Table 1) decreases at a much smaller rate at increasing frequencies (18).

The RF field inhomogeneity poses a serious challenge for high-field MRI applications. Phantom designs that simulate RF field wave behavior in the human body are critical for devising imaging methods and new coil designs to address this problem (13,15,25,26). The development of phantoms will be valuable in the development of parallel imaging methods for high-field MRI systems. The experiments at 7.0 T demonstrate that parallel-imaging methods that utilize inhomogeneous RF fields for spatial encoding would most likely offer a solution to this problem (25,27). The development and optimization of parallel imaging methods and multicoil systems for high fields require phantoms that closely simulate the RF field behaviors of a specific coil design in the human body. The methods and results of this study represent an important step toward developing phantoms that are suitable for high-field MRI. Based on the principles demonstrated with this method, more deliberate phantoms can be devised for evaluations of parameters that are influenced by RF field wave behaviors, such as image SNR and tissue SAR distributions, and the loading effect of RF coil systems at various field strengths.

CONCLUSIONS

In the presence of wave behavior at high field, the RF field distribution inside a sample of an RF coil depends on the field strength and sample electromagnetic properties. To design a phantom for a high-field human imaging system, one must scale the phantom size and skin-depth with the RF field wavelength in the sample. We demonstrated experimentally with various RF coils at 7.0 T that the phantom designed with our method closely approximated the image intensity distribution in a human head, despite the heterogeneous distributions of σ and ϵ_r , and the complicated geometry of the biological samples.

This phantom design method can be utilized for comparing and predicting image signal distributions of an RF coil configuration at different field strengths. The experimental results at 7.0 T and 3.0 T validated our method. With this method, we were able to predict the image intensity distribution in a human head at 9.4 T, using an experimental image with a 7.0 T equivalent phantom.

REFERENCES

- Turner R, Jezzard P, Wen H, Kwong KK, Bihan DL, Zeffiro T, Balaban RS. Functional mapping of the human visual cortex at 4 and 1.5 Tesla using deoxygenation contrast EPI. *Magn Reson Med* 1993;29:277–279.
- Hen H, Denison TJ, Singerman RW, Balaban RS. The intrinsic signal to noise ratio in human cardiac imaging at 1.5, 3, and 4 T. *J Magn Reson* 1997;125:65–71.
- Ordidge RJ, Gorell JM, Deniau JC, Knight RA, Helpert JA. Assessment of relative brain iron concentrations using T_2 -weighted and T_2^* -weighted MRI at 3 Tesla. *Magn Reson Med* 1994;32:335–341.
- Ugurbil K, Hu X, Chen W, Zhu XH, Kim SG, Georgopoulos A. Functional mapping in the human brain using high magnetic fields. *Phil Trans R Soc Lond B Biol Sci* 1999;35:1195–213.
- Chen W, Ugurbil K. High spatial resolution functional magnetic resonance imaging at very-high-magnetic field. *Top Magn Reson Imaging* 1999;10:63–78.
- Hoult DI, Phil D. Sensitivity and power deposition in a high-field imaging experiment. *J Magn Reson Imaging* 2000;12:46–67.
- Yacoub E, Shmuel A, Pfeuffer J, Moortele P, Adriany G, Anderson P, Vaughan JT, Merkle Hellmut, Ugurbil K, Hu X. Imaging brain function in humans at 7 Tesla. *Magn Reson Med* 2001;45:588–594.
- Yang QX, Smith MB, Zhu X, Liu H, Michaeli S, Zhang X, Anderson P, Adriany G, Merkle H, Ugurbil K, Chen W. T_2^* -weighted human brain imaging with the GESEPI at 7.0 Tesla. In: Proceedings of the 8th Annual Meeting of ISMRM, Denver, 2000. p 1684.
- Robitaille PM, Abduljalil AM, Kangaru A. Ultra high resolution imaging of the human head at 8 tesla: 2K x 2K for Y2K. *J Comput Assist Tomogr* 2000;24:2–8.
- Collins CM, Smith MB. Signal-to-noise ratio and absorbed power as functions of main magnetic field strength, and definition of “90°” RF pulse for the head in the birdcage coil. *Magn Reson Med* 2001;45:684–691.
- Vaughan JT, Garwood M, Collins CM, Liu W, DelaBarre L, Adriany G, Andersen P, Merkle H, Goebel R, Smith MB, Ugurbil K. 7T vs. 4T: RF power, homogeneity, and signal-to-noise comparison in head images. *Magn Reson Med* 2001;46:24–30.
- Glover GH, Hayes CE, Pelc NJ, Edelstein WA, Mueller OM, Hart HR, Hardy CJ, O'Donnell M, Barber WD. Comparison of linear and circular polarization for magnetic resonance imaging. *J Magn Reson* 1985;64:255–270.
- Foo TK, Hayes C, Kang YW. Reduction of RF penetration effects in high field imaging. *Magn Reson Med* 1992;23:287–301.
- Tofts PS. Standing waves in uniform water phantoms. *J Magn Reson Ser B* 1994;104:134–147.
- Alsop DC, Connick TJ, Mizsei G. A spiral volume coil for improved RF field homogeneity at high static magnetic field strength. *Magn Reson Med* 1998;40:49–54.
- Jin J, Chen J. On the SAR and field inhomogeneity of birdcage coils loaded with the human head. *Magn Reson Med* 1997; 38:953–63.
- Ibrahim TS, Lee R, Baertlein BA, Robitaille PM. B_1 field homogeneity and SAR calculations for the birdcage coil. *Phys Med Biol.* 2001;46:609–619.
- Yang QX, Wang JH, Collins CM, Smith MB, Zhang X, Liu H, Michaeli S, Zhu X-H, Adriany G, Vaughan JT, Anderson P, Ugurbil K, Chen W. Analysis of wave behavior in dielectric sample at high field. *Magn Reson Med* 2002;47:982–989.
- Wang JH, Yang QX, Collins CM, Smith MB, Zhang X, Liu H, Zhu X-H, Adriany G, Ugurbil K, Chen W. The polarization of the radiofrequency field in a human head at high field: a study with a quadrature surface coil at 7.0 Tesla. *Magn Reson Med* 2002;48:362–369.
- Johnk CT. Engineering electromagnetic fields and waves. New York: Wiley; 1988. p 363.
- Gabriel C. Compilation of the dielectric properties of body tissues at RF and microwave frequencies. Air Force materiel command, Brooks Air Force Base, Texas: AL/OE-TR-1996-0037; 1996.
- Hartsgrove G, Kraszewski A, Surowiec A. Simulated biological materials for electromagnetic radiation absorption studies. *Bioelectromagnetics* 1987;8:29–36.
- Beck BL, Jenkins KA, Cocca JR, Simmons F. Tissue-equivalent phantoms for high frequencies. *Concepts Magn Reson B* 2004;20B:30–33.
- Vaughan JT, Hetherington HP, Otu JO, Pan JW, Pohost GW. High frequency volume coils for clinical NMR imaging and spectroscopy. *Magn Reson Med* 1994;32:206–218.
- Adriany G, Van de Moortele P, Wiesinger F, Andersen P, Strupp J, Zhang X, Snyder CJ, Chen W, Pruessmann KP, Boesiger P, Vaughan JT, Ugurbil K. Transceive stripline arrays for ultra high field parallel imaging applications. In: Proceedings of the 11th Annual Meeting of ISMRM, Toronto, Canada, 2003. p 474.
- Saekho S, Boada FE, Noll DC, Stenger VA. B_1 inhomogeneity compensation using 3D tailored RF pulses. In: Proceedings of the 11th Annual Meeting of ISMRM, Toronto, Canada, 2003. p 717.
- Beck BL, Jenkins KA, Padgett K, Fitzsimmons JR, Blackband SJ. Observation of B_1 inhomogeneities on large biological samples at 11.1 Tesla. In: Proceedings of the 11th Annual Meeting of ISMRM, Toronto, Canada, 2003. p 716.